Single-Sideband OFDM Transmission via a Silicon Microring IQ Modulator

Mingyang Lyu, Yelong Xu, Leslie A. Rusch and Wei Shi

IEEE Photonics Technology Letters, (Volume 31, Issue 2) (2018)

Doi: 10.1109/LPT.2018.2886557

https://ieeexplore.ieee.org/abstract/document/8574993

Single-Sideband OFDM Transmission via a Silicon Microring IQ Modulator

Mingyang Lyu, *Student Member, IEEE,* Yelong Xu, *Member, IEEE,*
Leslie A. Rusch, *Fellow, IEEE,* and Wei Shi, *Member, IEEE*

***Abstract*—We experimentally demonstrate the generation of a single-sideband orthogonal frequency division multiplexed (OFDM) signal using an on-chip silicon photonics microring-based IQ modulator. Over 18 dB sideband suppression ratio is achieved for the wideband OFDM: 15.7 GHz data band and 2.7 GHz guard band. The 31.4 Gb/s signal was transmitted over 20 km of standard single-mode fiber with a bit error rate below the forward error correction threshold. While single-sideband continuous-wave signals have been produced with such hardware, this is the first demonstration of stable data transmission on the single sideband carrier.**

***Index Terms*—Silicon Photonics, Single Side-band, OFDM, Microring Modulator**

I. Introduction

PASSIVE optical networks (PONs) accomplish high-bandwidth Internet delivery by taking advantage of low loss optical fiber and simple on/off keying transceivers. As new video streaming and mobile services push the need for greater PON bandwidth, we need cost-effective hardware to work with advance modulation to increase throughput. That modulation should remain compatible with simple direct detection schemes currently in use. The point-to-multipoint PON architecture provides an efficient access network that could be complimented with emerging silicon photonic components.

The major short-reach PON constraints are implementation cost and flexibility. Orthogonal frequency division multiplexing (OFDM) is attractive for PONs owing to its flexibility in sculpting both time and frequency resources. To maintain low cost and simplicity, direct detection (DD) OFDM is widely considered for future PONs [1]. Link performance is limited by chromatic dispersion (CD), which results in destructive interference between two sidebands of double sideband (DSB) OFDM modulation. It causes severe frequency-related power fading, especially for wider band signal and longer distances [2]. Single sideband (SSB) OFDM modulation avoids the power fading and doubles the potential spectral efficiency. SSB-OFDM modulation can be realized by directly filtering the undesired sideband [3], but requires sharp filters with well controlled center frequency to isolate one sideband precisely. External modulators [4], such as dual-drive Mach-Zehnder modulators (MZM) and optical in-phase and quadrature (IQ) modulators, can generate SSB signals. Integrated versions of these modulators provide a more affordable solution.

Silicon photonics (SiP) is a CMOS-compatible technology based on high-index-contrast waveguides, that can be used for high-speed optical modulators [5]. Compared to MZMs, microring modulators (MRMs) [6] have the advantage of ultra-small footprint and low power consumption (down to fJ/bit), both superb attributes for short-reach applications. A microring IQ modulator was demonstrated for QAM modulation with coherent detection [7]. Single-sideband OFDM (with waterfilling) was experimentally demonstrated in [8] using a silicon IQ MZM. A single-chip MRM based optical SSB modulator was demonstrated in [9], but only for sinusoidal signals. Wideband SSB-OFDM transmission using an MRM, to the best of our knowledge, has not been reported until this time.

In this letter, we use a silicon microring IQ modulator to generate an optical SSB signal for a direct detection system. We demonstrate the generation of flat, wideband (15.7 GHz) SSB-OFDM with a 2.7 GHz guard band for a total covered bandwidth of 18.4 GHz. The sideband suppression ratio is larger than 18 dB. Transmission over a 20 km standard single mode fiber (SSMF) is presented, with a measured bit error rate well below the 7% overhead forward error correction (FEC) threshold. We discuss how this subsystem could enable upgraded data rates, as well as new services for PON systems.

II. Device Design and Characterization

We designed a microring IQ modulator on the silicon-on-insulator (SOI) platform. As shown in Fig. 1, two identical MRMs modulators (MRM1 and MRM2) are loaded in a balanced Mach-Zehnder interferometer (MZI). The $\pi/2$ phase shift between the branches allows operation of the modulators for complex (IQ) modulation. The phase shift tuning is implemented by a 100 μm N++/N/N++ resistor-based heater.

Each MRM has a radius of 20 μm, a coupling gap of 180 nm, an all-pass structure and are overcoupled. They

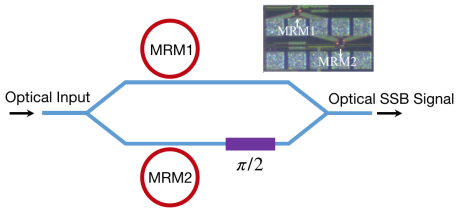

Fig. 1. Schematic and microscope image of an optical SSB transmitter based on silicon microring IQ modulator.

This work is supported by Fonds de Recherche du Qubec-Nature et Technologies (FRQNT) (2016-NC-190737), National Science and Engineering Research Council of Canada (NSERC) (CRDPJ499664), PROMPT Quebec grant (52_Rusch 2016.09), TELUS and Aeponyx.

Mingyang Lyu, Yelong Xu, Leslie A. Rusch and Wei shi are with Centre for Optics, Photonics, and Lasers (COPL), ECE department, Université Laval (e-mail: mingyang.lyu.1@ulaval.ca, yelong.xu.1@ulaval.ca, leslie.rusch@gel.ulaval.ca, wei.shi@gel.ulaval.ca).

National Science and Engineering Council of Canada (NSERC) Funding: CRDPJ/499664-2016

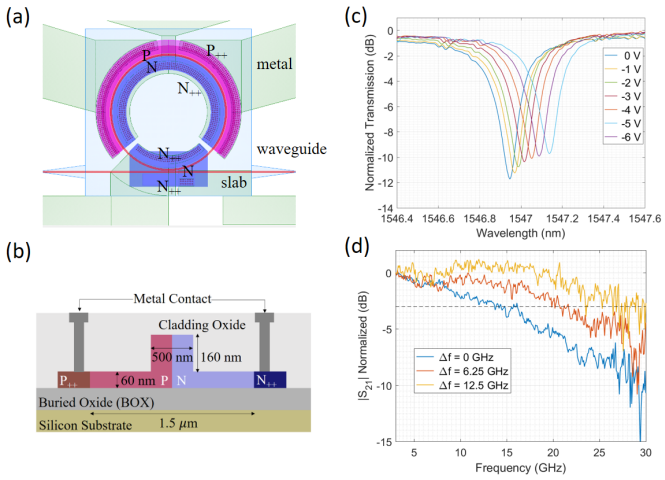

Fig. 2. (a) Partial mask layout for MRM1/MRM2, (b) cross section of the p-n junction of MRM1/MRM2 showing relevant dimensions, for MRM1 measured (c) power transmission spectra at different bias voltages, and (d)electro-optic frequency response (S21) at different frequency detunings.

exploit the plasma dispersion effect through carrier depletion in a lateral p-n junction. The p-n junction for intracavity modulation spans roughly 70% of the circumference, whereas the N++/N/N++ resistor-based heater for wavelength tuning spans roughly 20% of the circumference, as shown in the partial mask layout in Fig. 2a. The cross section of the waveguide phase shifter is shown in Fig. 2b. The silicon waveguide has a rib thickness of 220 nm with a 60 nm thick slab used for electrical connections. The device was fabricated in a multi-project-wafer run at IMEC, Belgium. Bond pad for RF probing dominate the 0.69 mm $\times$ 0.41 mm footprint.

The measured optical transmission spectra of MRM1 for various bias voltages are presented in Fig. 2c. The MRM exhibits a resonance depth of around 10.8 dB at zero bias. The depth decreases as the reverse potential increases, indicating an overcoupling condition in reverse bias. The resonance shift as a function of reverse bias voltage shows an efficiency of about 2 GHz/V. The measured free spectral range (FSR) is 4.78 nm and the quality factor at equilibrium is 8320. Frequency detuning Δf, defined as the difference between the optical input frequency and the cavity resonant frequency. The measured MRM1 electro-optic, S21, response at -2 V bias is reported in Fig. 2d for various detunings; 3 dB bandwidth is greater than 25 GHz at -2 V bias for 12.5 GHz detuning.

III. Experimental Setup

The experimental setup is illustrated in Fig. 3. The Cobrite external cavity laser (100 kHz linewidth) was tuned to 1550.5 nm and coupled to the chip with a 250 μm spaced fiber array via polarization maintaining fiber. A 23-order pseudo random bit sequence (PRBS) was mapped to QPSK and OFDM coded (details in next section). Only positive subcarriers (higher frequency than the optical carrier) are non-zero, i.e., single-side-band OFDM in the electrical domain. The OFDM IQ values are fed to two channels of an 84 GS/s digital-to-analog converter (DAC) with 16 GHz bandwidth and 8-bit resolution. The driving signals generated by the DAC are amplified by two cascaded 50 GHz RF amplifiers.

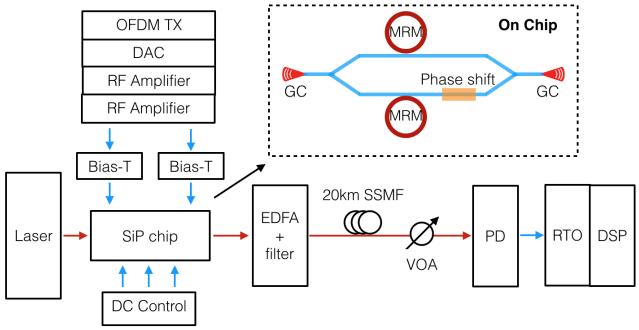

Fig. 3. Experimental Setup

The two MRMs on chip are driven via a GSGSG configured, 50 Ω-terminated, 50 GHz microprobe. The two rings are heated to change the offset between the resonance peak and laser wavelength. The waveguide in the lower branch of the MZI is also heated to generate a 0.5π phase difference between the two arms of the IQ modulator with a DC driving voltage of $\sim$1.3 V. An EDFA boosts chip output power. A tunable optical band pass filter (OBPF) with a 0.4 nm passband bandwidth removes out-of-band amplified spontaneous-emission noise. After 20 km SSMF propagation, a variable optical attenuator (VOA) sweeps received power to a photodetector with a transimpedance amplifier. The electrical signal is captured at 80 GSa/s by a real-time oscilloscope (RTO) with 30 GHz analog bandwidth.

IV. Experimental Results

A. Generated SSB-OFDM signal

The OFDM signal is generated off-line in Matlab. The IQ modulator uses complex data to produce a single side-band version in the optical domain. The dark grey curve in Fig. 4 shows the optical spectrum of the SSB-OFDM signal before transmission. The left sideband is well suppressed by IQ modulation, with sideband suppression ratio greater than 18 dB. The OSNR is limited by electrical driving signals. The cascaded amplifiers are suboptimal, but required due to equipment availability. The weak DAC electrical output (50 mV peak-to-peak amplitude) was amplified to 5 V_{pp}. The degraded electrical SNR leads to an OSNR of approximately 18 dB. The residual sideband is almost totally buried by the noise. Small distortions near the carrier and after the OFDM band are due to DAC imperfections.

The data was QPSK modulated and parsed into blocks of 191 symbols. The symbols were zero padded to form a block of length 1024, corresponding to the total number of subcarriers. The FFT length of 1024 covers 84 GHz (DAC sampling rate of 84 GS/s), for a subcarrier bandwidth of 82 MHz. The suppressed sideband is a result of the 512 lower subcarriers being zeroed out. We allocated 33 subcarriers (2.7 GHz) as a guard band, so the 191 data subcarriers (15.7 GHz) were followed by 288 zero subcarriers at the highest frequencies. The guard band avoids severe signal-to-signal beat interference (SSBI) at baseband; for more spectral efficiency, a Kramer-Kronig receiver [10] could be used without a guard band.

National Science and Engineering Council of Canada (NSERC) Funding: CRDPJ/499664-2016

The upper frequencies were unused due to the bandwidth of the MRMs. Per measurements in Fig. 2, the 3 dB bandwidth of the MRM is around 23 GHz. A section of 6.25% of the signal was appended as a cyclic prefix to increase the dispersion tolerance. Linear pre-emphasis was used to balance the non-flat DAC response, and uniform subcarriers are observed in the optical spectrum in Fig. 4. The slight notch comes from the imperfect DAC frequency response, which leads to the poor performance of the middle subcarrier to be seen later in Fig. 6.

In [9], a single sideband sinusoidal signal is presented within a 5 GHz range, so wideband modulation of the sideband was not examined. The MRM has inherent frequency selectivity. On the positive side, we can cascade ring-based IQ modulators to realize modulation of wavelength division multiplexing (WDM) signals without additional filters as discussed in section V. However, at the same time, the MRM filtering effect imposes a frequency roll-off on the modulated signal. As the overall performance of OFDM transmission is limited by the worst subcarrier, it is important to maintain uniform performance of all subcarriers. In wide-band signal generation, the roll-off will result in worse performance for higher frequency components. To compensate the response of MRMs, pre-emphasis can be used to balance the subcarrier performance. However, too strong pre-emphasis degrades the overall performance, ultimately limiting bandwidth.

Fig. 5 shows the received electrical spectrum after 20 km SSMF transmission. In Fig. 5a the transmitted signal was SSB-OFDM with spectrum in Fig. 4. In Fig. 5b the transmitted signal was instead DSB-OFDM signal with the same number of subcarriers and guard band. For both cases, the received power is adjusted to -1 dBm using a VOA. The advantage of SSB modulation is clearly visible: the SSB-OFDM signal shows a flat spectrum, while the DSB-OFDM signal has severe attenuation in frequencies near the optical carrier due to the chromatic-dispersion-induced nonlinear phase response. This results in strong fading of DSB-OFDM after direct detection. An inset shows the constellation of the last subcarrier for each case. The DSB-OFDM constellation is noisier than the SSB-OFDM signal due to interference. As ring modulators are resonant structures, phase shift is frequency dependent. The single phase compensation for the whole band leads to residual phase shift at the last subcarrier, hence the visible constellation rotation.

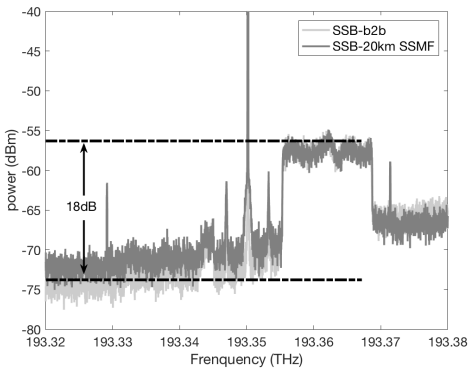

Fig. 4. Optical spectrum of SSB-OFDM signal before transmission in dark grey and after 20 km transmission in light grey.

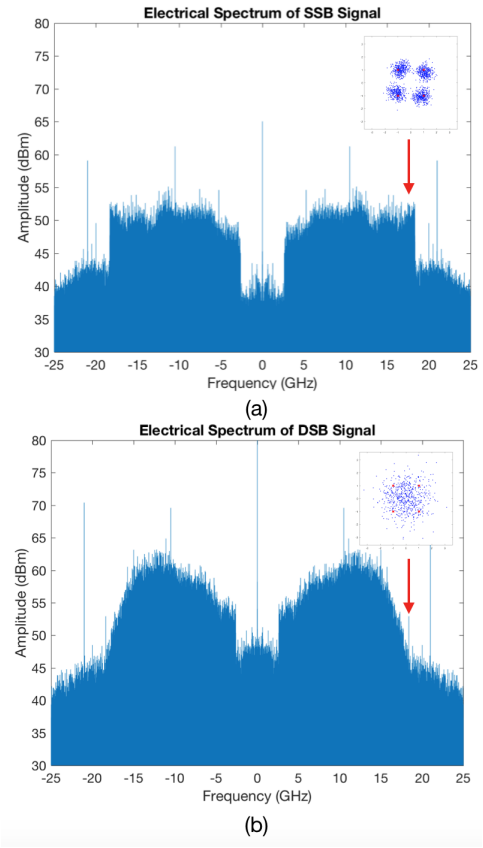

Fig. 5. Received electrical spectrum and constellations for after transmission over 20 km of SSMF of (a) SSB-OFDM signal of Fig. 4, and (b) a DSB-OFDM signal;insets show constellation of subcarrier number 191.

B. BER performance

We generate a PRBS sequence off-line in Matlab. The sequence is mapped on 191 subcarriers to generate 10,000 QPSK OFDM symbols per frame. Zeros are padded to form the final frame with a length of 2^{22}. In each detection, the frame is captured five times and the counted errors are averaged for higher precision.

We find the BER performance for DSB and SSB signals to highlight the improvement with efficient SSB generation. We calculate the BER per subcarrier; frequency-dependent impairments are clearly eliminated with SSB. We estimate SNR from BER and plot the estimated SNR per subcarrier in Fig. 6. Performance is uniform over all subcarriers after the 20 km SSMF in the solid (blue) curve for SSB-OFDM in Fig. 6. The small notch comes from DAC imperfections for both SSB and DSB signal. The overall estimated BER is 2.75×10^{-3}, well below the 7% FEC threshold (3.8×10^{-3}). In the dashed (red) curve for DSB-OFDM in Fig. 6 we can see clear fading due to chromatic dispersion. As the overall performance is dominated by the worst subcarriers, the performance of DSB sees a significant degradation; the overall counted BER for DSB-OFDM is 2.6×10^{-2}.

The transmission performance of SSB-OFDM signal over a range of receiving power is shown in Fig. 7. We use the 7% FEC threshold as a reference. The BER increases smoothly as the received power drops. For a received power larger than -4 dBm, we achieve error-free transmission.

National Science and Engineering Council of Canada (NSERC) Funding: CRDPJ/499664-2016

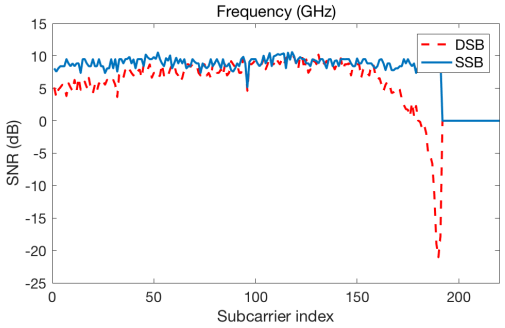

Fig. 6. Estimated SNR per subcarrier for SSB signal (solid blue curve) and DSB signal (dashed red curve)

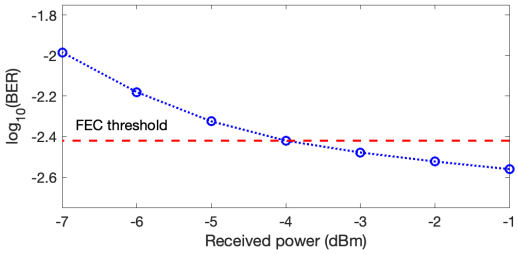

Fig. 7. BER of detected SSB-OFDM signal with varied received power.

The optical spectrum of the generated SSB-OFDM signal after 20 km SSMF is shown in the dark grey curve in Fig. 4. The spectrum remains uniform after transmission while the left side band is totally buried by the noise. The OSNR decreases due to the fiber loss, which limits the performance. The OSNR in this demonstration is limited by the poor electrical signal quality. Better performance can be achieved with a higher output power DAC or low-noise RF amplifiers.

C. Discussion

MRMs are inherently frequency selective. Using MRMs at the customer premises could enable WDM on current PON infrastructures without deploying array waveguide gratings (AWGs). A colorless solution [11] could be achieved by tuning the MRM center frequency at the customer premises.

MRMs could also be effective at the central office for generation of WDM signals. Both paths of the IQ modulator could incorporate multiple MRMs in a cascade sharing the same single bus. With a comb source input, different sets of MRMs can be thermally tuned to the frequencies of the comb lines and modulate the tones. As shown in Fig. 2, the bandwidth of the MRM is around 0.2 nm, significantly smaller than the typical WDM grid (0.8 nm). Cascaded MRMs can be tuned to create 0.8 nm frequency drift between adjacent MRMs. For every set of MRMs, only one tone is modulated; other tones, as well as the modulated signal (within 0.2 nm range to tones),are out of band and unaffected.

MRMs could also enable new PON services. By designing MRMs with higher Q factors, we can realize very narrow bandwidth MRMs to support radio over fiber (RoF) multiplexing. An MRM with confined operation bandwidth allows us to add several downlink RoF channels onto tightly spaced wavelengths falling within a single WDM slot. Single sideband RoF signals could be generated via the IQ structure to achieve a doubled spectral efficiency and thus higher flexibility in wavelength. While MRMs are sensitive to fabrication tolerance and environmental temperature, this can be addressed using feedback control [12].

V. Conclusion

We demonstrated, for the first time, the generation of wide-band optical SSB-OFDM over a 15.7 GHz bandwidth with a 2.7 GHz guard band, using an integrated silicon microring IQ modulator. The side-band suppression ratio is 18 dB over a wide range. Performance and robustness against chromatic dispersion is examined via transmission of 20-km SSMF. A raw data rate of 31.3 Gb/s with a 6.25 % cyclic prefix has been achieved. This subsystem provides a low-cost integrated solution for SSB signal transmitters. The frequency selectivity and tunability allows colorless operation in next-generation PONs. This solution is also compatible with WDM without additional equipment such as wavelength (de-)multiplexers.

Acknowledgement

We thank CMC Microsystems for the fabrication subsidy and multi-project wafer service.

References

[1] J.-I. Kani, F. Bourgart, A. Cui, A. Rafel, M. Campbell, R. Davey, and S. Rodrigues, "Next-generation pon-part i: Technology roadmap and general requirements," IEEE Communications Magazine, vol. 47, no. 11, pp. 43–49, 2009.

[2] G. Meslener, "Chromatic dispersion induced distortion of modulated monochromatic light employing direct detection," IEEE Journal of Quantum Electronics, vol. 20, no. 10, pp. 1208–1216, 1984.

[3] L.-S. Yan, C. Yu, Y. Wang, T. Luo, L. Paraschis, Y. Shi, and A. Willner, "40-gb/s transmission over 25 km of negative-dispersion fiber using asymmetric narrow-band filtering of a commercial directly modulated dfb laser," IEEE photonics technology letters, vol. 17, no. 6, pp. 1322–1324, 2005.

[4] G. H. Smith, D. Novak, and Z. Ahmed, "Overcoming chromatic-dispersion effects in fiber-wireless systems incorporating external modulators," IEEE transactions on microwave theory and techniques, vol. 45, no. 8, pp. 1410–1415, 1997.

[5] W. Shi, Y. Xu, H. Sepehrian, S. LaRochelle, and L. A. Rusch, "Silicon photonic modulators for PAM transmissions," Journal of Optics, vol. 20, no. 8, p. 083002, 2018.

[6] R. Dubé-Demers, S. LaRochelle, and W. Shi, "Ultrafast pulse-amplitude modulation with a femtojoule silicon photonic modulator," Optica, vol. 3, no. 6, pp. 622–627, 2016.

[7] P. Dong, C. Xie, L. Chen, N. K. Fontaine, and Y.-k. Chen, "Experimental demonstration of microring quadrature phase-shift keying modulators," Optics letters, vol. 37, no. 7, pp. 1178–1180, 2012.

[8] C. Y. Wong, S. Zhang, Y. Fang, L. Liu, T. Wang, Q. Zhang, S. Deng, G. N. Liu, and X. Xu, "Silicon iq modulator for next-generation metro network," Journal of Lightwave Technology, vol. 34, no. 2, pp. 730–736, 2016.

[9] B.-M. Yu, J.-M. Lee, C. Mai, S. Lischke, L. Zimmermann, and W.-Y. Choi, "Single-chip si optical single-sideband modulator," Photonics Research, vol. 6, no. 1, pp. 6–11, 2018.

[10] Z. Li, M. S. Erkılınç, K. Shi, E. Sillekens, L. Galdino, B. C. Thomsen, P. Bayvel, and R. I. Killey, "Ssbi mitigation and the kramers–kronig scheme in single-sideband direct-detection transmission with receiver-based electronic dispersion compensation," Journal of Lightwave Technology, vol. 35, no. 10, pp. 1887–1893, 2017.

[11] R. Urata, C. Lam, H. Liu, and C. Johnson, "High performance, low cost, colorless onu for wdm-pon," in National Fiber Optic Engineers Conference. Optical Society of America, 2012, pp. NTh3E–4.

[12] P. Dong, R. Gatdula, K. Kim, J. H. Sinsky, A. Melikyan, Y.-K. Chen, G. De Valicourt, and J. Lee, "Simultaneous wavelength locking of microring modulator array with a single monitoring signal," Optics Express, vol. 25, no. 14, pp. 16 040–16 046, 2017.

National Science and Engineering Council of Canada (NSERC) Funding: CRDPJ/499664-2016